J. Electrochem. Sci. Eng. **16** (2026) 2875; http://dx.doi.org/10.5599/jese.2875

Open Access : ISSN 1847-9286
https://pub.iapchem.org/ojs/index.php/JESE

Original scientific paper

Synergistic Ni-Co interaction and phase control in bimetallic catalyst for ethanol electrooxidation reaction

Muhammad Fathar Aulia[1], Abdul Asywalul Fazri[2], Suci Winarsih[3], Mohammad Hamzah Fauzi[3], Jumaeda Jatmika[3] and Setia Budi[2,✉]

[1]*The Center for Science Innovation, Arva Building, Jl. RP. Soeroso, Jakarta Pusat 10350, Indonesia*
[2]*Department of Chemistry, Faculty of Mathematics and Natural Sciences, Universitas Negeri Jakarta, Jl. Rawamangun Muka, Jakarta 13220, Indonesia*
[3]*Research Center for Quantum Physics, National Research and Innovation Agency (BRIN), South Tangerang 15314, Indonesia*
Corresponding authors: ✉setiabudi@unj.ac.id

Received: July 4, 2025; Accepted: September 30, 2025; Published: October 12, 2025

Abstract

In this study, bimetallic nickel-cobalt electrocatalysts with different Ni:Co ratios were electrodeposited onto indium tin oxide substrates coated by polyethylene terephthalate and evaluated as cost-effective catalysts for ethanol electrooxidation reaction. The physical features of the catalysts were studied using X-ray diffraction (XRD), Raman spectroscopy and field-emission scanning electron microscopy, along with energy-dispersive X-ray spectroscopy. XRD analysis revealed a phase transition from a mixed face-cantered cubic (FCC) and hexagonal close-packed structure to a single FCC phase, as the cobalt content decreased. This change in phases greatly affected the shape of the catalyst, changing from a pebbly texture in the mixed-phase samples to a smooth, rounded shape in the single-phase FCC samples. The electrochemical properties and catalytic performance of ethanol oxidation in alkaline medium were investigated using cyclic voltammetry and electrochemical impedance spectroscopy. The tested electrocatalysts revealed that NiCo B having Ni:Co ratio 82:18 possess the best catalytic activity compared to the other catalysts, reaching a current density of 14.82 mA cm^{-2} for ethanol electrooxidation reaction and showing great stability. This better performance is due to its improved physical structure, which boosts the interaction between nickel and cobalt, and lowers resistance to charge transfer. These findings demonstrate the promise of NiCo as an efficient electrocatalyst for ethanol electrooxidation reaction.

Keywords

Ni-Co electrocatalysts; electrodeposition; thin films; phase transition; direct alcohol fuel cells

Introduction

Direct alcohol fuel cells (DAFCs) have attracted considerable interest due to their higher energy conversion efficiency, abundant energy supply, simplified system design and ability to operate

without high pressure or temperature [1]. Ethanol is considered a viable alternative to alcohol because of its less toxic characteristics and higher theoretical energy density in comparison with methanol [2]. In addition, ethanol offers a number of advantages such as affordability, ease of management, convenient to transport and storage, and can produced from renewable energy sources [3]. Ethanol is converted into electrical energy through the cleavage of its C-C bonds, ideally providing 12 e^- and CO_2 [4]. However, the electrooxidation of ethanol at the anode occurs with slow kinetics, frequently leading to partial oxidation [5]. Consequently, ethanol is generally oxidised to acetic acid or acetaldehyde and just providing 2 or 4 e^- [6]. Improving this sluggish electrooxidation process necessitates the utilisation of electrocatalysts. Platinum is considered the most efficient electrocatalyst for the ethanol electrooxidation reaction (EOR) [7]. Nonetheless, their elevated expense is a considerable obstacle to the commercial feasibility of DEFCs [8]. Furthermore, these noble metal catalysts demonstrate restricted long-term durability and are particularly susceptible to CO poisoning, which considerably limits their total catalytic efficacy [9].

Among the various non-noble metals, nickel (Ni) has attracted considerable attention owing to its advantageous surface characteristics and modest inherent activity for ethanol oxidation [10]. In alkaline environments, Ni demonstrates favourable electrocatalytic properties by establishing active $Ni(OH)_2$/NiOOH redox couple, which promotes ethanol oxidation and improves kinetics *via* formation of high-valent nickel species [11]. Nonetheless, despite its affordability and availability, pure nickel catalysts frequently demonstrate restricted catalytic performance and inadequate long-term stability, principally attributable to surface passivation by insulating hydroxide layers and poisoning by carbonaceous intermediates [12].

Extensive efforts have been focused on structural and compositional adjustments to overcome these limitations. In this regard, bimetallic Ni-based systems (Ni-M; M = Cu [13], Mn [14] and Co [15]) have been widely studied. Ni-Co alloys exhibit significant promise; whereas cobalt (Co) alone shows limited EOR activity, its integration into Ni produces a synergistic effect [16]. This improvement is due to a bifunctional mechanism, in which Co reduces CO poisoning by enhancing OH^- adsorption at lower potentials, thus increasing the production of catalytically active NiOOH species and expediting the overall reaction kinetics [17]. This synergistic interaction promotes catalytic activity and improves the electrochemical stability of the system. The use of supplementary metal elements has been shown to improve both the catalytic performance and electrochemical stability of Ni-based EOR catalysts [18].

Nonetheless, despite these benefits, obstacles persist in completely enhancing the catalytic efficiency of Ni-Co systems. The catalytic activity is very sensitive to the composition and microstructure of the alloy layers. Consequently, additional study is necessary to systematically enhance the composition and structural attributes of Ni-Co films. The electrodeposition technique is a widely utilised approach for the synthesis of thin films and alloys [19,20]. This approach facilitates the generation of high-purity films with extensive surface areas and adjustable topological structures and morphologies, which are critical features in enhancing electrocatalyst performance for EOR [21]. Prior study indicates that their microstructure and shape are significantly influenced by cobalt composition, which may be regulated through deposition parameters [22].

Despite the availability of numerous papers on the electrodeposition of NiCo thin films, studies on the physical parameters related to their electrocatalytic properties are lacking. Therefore, this study systematically compares the phase transformation of the electrodeposited NiCo thin films with the EOR electrocatalytic activity. This study includes synthesis NiCo thin films which is electrodeposited on an indium tin oxide (ITO) coated by polyethylene terephthalate (PET) substrate by a potentiostatic electrodeposition method. The physical properties of these catalysts were

examined using X-ray diffraction (XRD), Raman spectroscopy and field emission scanning electron microscopy-energy dispersive X-ray (FESEM-EDX) while their electrocatalytic performance for ethanol oxidation in alkaline solution was investigated by electrochemical impedance spectroscopy (EIS) and cyclic voltammetry (CV).

Experimental

Materials

Chemicals used to synthesize NiCo thin films were nickel sulfate hexahydrate ($NiSO_4 \cdot 6H_2O$), cobalt sulfate heptahydrate ($CoSO_4 \cdot 7H_2O$), and boric acid (H_3BO_3), the materials were analytical grade chemicals supplied by Merck. The substrate used was indium tin oxide (ITO) coated by polyethylene terephthalate (PET) with a resistance of 10 Ω/square.

Synthesis of NiCo thin films

The E410 potentiostat controls the standard configuration of three electrodes for the synthesize of NiCo thin films at room temperature by potentiostatic electrodeposition. Indium tin oxide (ITO) substrate with a dimension of 2×1 cm and a deposition area of 1 cm^2 was used as working electrode, Pt wire as counter electrode and AgCl (3 M KCl) as reference electrode. PET substrates coated with ITO were selected for their excellent conductivity, flexibility and transparency, which provide an optimal platform for the single deposition of catalyst and efficient electrochemical analysis. Prior to deposition, the ITO substrate has been repeatedly washed with distilled water and ethanol. The solution of electrolytes (without stirring) used during the deposition is given in Table 1. Electrodeposition was performed at a constant potential of -1.5 V for 10 minutes at room temperature without adjusting the deposition pH. After that, the deposited samples were washed carefully with ethanol, and dried at room temperature [23].

Table 1. *Electrolyte composition for electrodeposition of NiCo thin films*

Samples	$NiSO_4 \cdot 6H_2O$ (M)	$CoSO_4 \cdot 7H_2O$ (M)	H_3BO_3 (M)
NiCo A	0.050	0.050	0.2
NiCo B	0.075	0.025	0.2
NiCo C	0.090	0.010	0.2

Physical characterization

The crystalline structure and phase of NiCo thin film were investigated by XRD using the Rigaku SmartLab (λ = 0.1541862 nm) with Cu K-alpha irradiation. Raman spectroscopy was carried out by LabRAM Aramis (Horiba Jobin Yvon) to investigate further the structure of the film. Surface morphology has been studied by field emission scanning electron microscopy (FESEM) using the JEOL Multibeam JIB 4610F system, which includes an energy-dispersive X-ray detector (EIS) for elemental determinations.

Electrocatalytic evaluation

Electrochemical evaluation of the NiCo thin films was carried out by CorrTest CS310 electrochemical workstation. A platinum plate was used as the counter electrode, and an Ag/AgCl electrode served as the reference electrode. Electrochemical impedance spectroscopy (EIS) measurements were taken from 100 kHz to 0.1 Hz at potential 0.6 V *vs.* Ag/AgCl to evaluate the charge transfer resistance. The electrocatalytic activity was tested using cyclic voltammetry (CV) over a potential range of −0.1 to 0.8 V compared to Ag/AgCl, with a scan rate of 250 mV s^{-1}. Linear sweep

voltammetry (LSV) analysis was performed over a potential range of -0.2 to 0.8 V *vs.* Ag/AgCl at a scan rate of 50 mV s^{-1}. To test the stability, chronoamperometric (CA) analysis was carried out for 2000 s at the potential 0.6 V. All electrochemical analyses were performed in 1 M NaOH containing 1 M ethanol. The measured potentials versus the Ag/AgCl reference electrode were converted to the reversible hydrogen electrode (RHE) using Equation (1) [24]:

$$E_{RHE} = E_{Ag/AgCl} + E^{o}_{Ag/AgCl} + 1.069\ pH \quad (1)$$

where E_{RHE} represents the converted potential *vs*. RHE, $E_{Ag/AgCl}$ is the experimentally measured potential against Ag/AgCl reference electrode and $E^{o}_{Ag/AgCl}$ = 0.197 V at 25 °C.

Results and discussion

Fig**ure** 1a displays the XRD patterns of the NiCo samples, showing clear peaks at 2θ = 44.4, 51.7 and 76.2° that match the (111), (200), and (220) crystal structures of the Ni-Co alloy (ICDD No. 01-074--5694) [25].

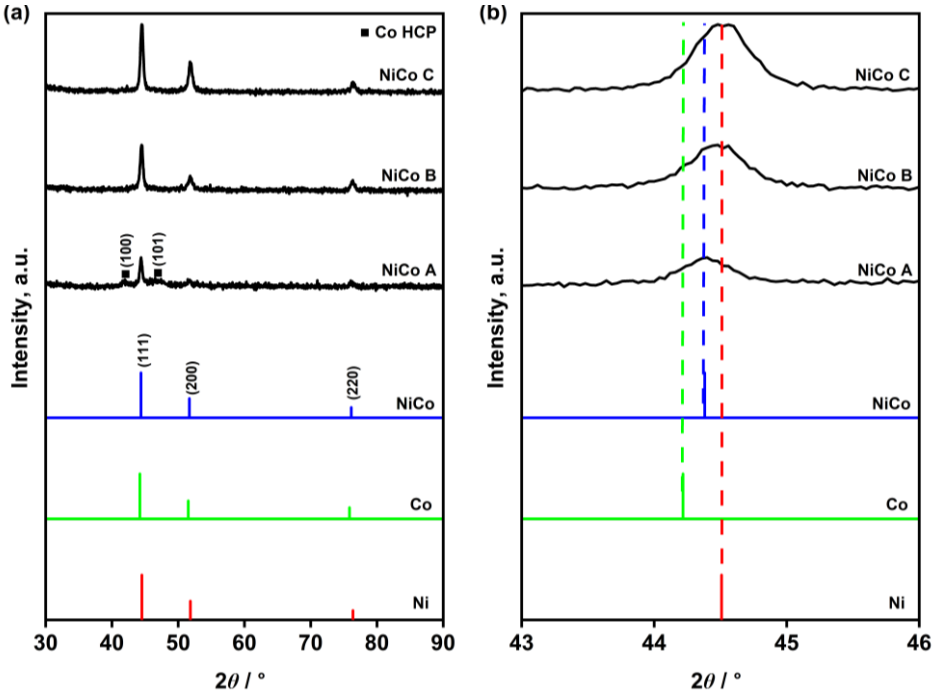

Figure 1. *(a) XRD patterns of NiCo thin films; (b) enlarged view around the (111) peak*

An enlarged view of the (111) peak, illustrated in Figure 1b, demonstrates that all observed peak positions are situated between those of pure Ni FCC (ICDD No. 00-004-0850) and Co FCC (ICDD No. 00-015-0806), thereby affirming the predominant formation of a Ni-Co alloy or the interaction between Ni and Co, in accordance with previous studies [26]. The diffraction peak changed to higher angles as the cobalt content diminished, potentially due to the partial substitution of Co with Ni [27]. To evaluate the preferred orientation of the structure, the texture coefficient (TC) was derived from the XRD pattern using the following Equation (2) [28]:

$$TC_{hkl} = \frac{I_{hkl} / I_{o\,hkl}}{1/N \sum_{n} I_{hkl} / I_{o\,hkl}} \quad (2)$$

where I_{hkl} is the relative intensity of a plane experimentally measured for the specified plane, $I_{o\,hkl}$ is the standard intensity of the same plane taken from the reference, N is the total number of reflections, and n is the number of diffraction peaks. The calculated values for the observed planes are shown in Table 2.

Table 2. *Texture coefficient of NiCo thin films*

Plane	TC		
	NiCo A	NiCo B	NiCo C
111	0.56	0.64	0.73
200	0.81	0.82	0.99
220	1.63	1.54	1.28

In the case of NiCo A, extra diffraction peaks at 2θ = 41.8 and 45.6°, which relate to the (100) and (101) planes, show that there is a hexagonal close-packed (HCP) cobalt phase [29]. The observed peaks are indicative of pure cobalt or cobalt-rich NiCo alloys with a hexagonal close-packed (HCP) structure, implying that NiCo A possesses a dual-phase structure comprising both HCP and face-centered cubic (FCC) phases. This arrangement is probably due to cobalt separating during the electrodeposition process, where areas rich in cobalt tend to form HCP-like NiCo alloys [30]. As the amount of Co decreases, the XRD patterns of NiCo B and NiCo C show no HCP-related peaks, meaning the HCP phase is not present. These samples exhibit solely FCC-related peaks, indicating the incorporation of Co atoms into the Ni lattice. The phase behaviour of the Ni-Co system is contingent upon composition, allowing for the existence of both FCC and HCP structures [31]. The phase structure of the bimetallic NiCo catalysts is significantly affected by the cobalt contents in the deposited films, as illustrated in Figure 3. The changes in phases match the Ni-Co phase diagram, showing that the FCC structure is stable when there is less cobalt and at normal temperatures [32]. The values of d-spacing and lattice constants were obtained using Equations (3) and (4) :

$$n\lambda = 2d_{hkl}\sin\theta \quad (3)$$

$$d_{hkl} = \frac{a}{\sqrt{h^2 + k^2 + l^2}} \quad (4)$$

where a denotes lattice constants, d = atomic plane spacing, λ = wavelength (0.15406 nm), (h, k, l) are Miller indices, and θ is incident angle. The d-spacing values determined in this study strongly align with the standard data set for NiCo, as presented in Table 3, and correspond accurately with the (111), (200) and (220) planes. The lattice parameter (a) of the FCC phase was derived from the XRD data, with the values for all samples presented in Table 3. The lattice parameters approximate those of the bulk material, exhibiting a little variation from 0.353452 to 0.352544 nm, attributable to alterations in the chemical composition of the NiCo thin films [33].

The crystallite size (D), the density of dislocation (δ), and the microstrain (ε) of all samples were determined from the (111) peak using Equations (5) to (7), respectively [34,35]:

$$D = \frac{0.9\lambda}{\beta\cos\theta} \quad (5)$$

$$\delta = \frac{1}{D^2} \quad (6)$$

$$\varepsilon = \frac{\beta}{4\tan\theta} \quad (7)$$

where λ denotes the wavelength of the X-ray employed for diffraction, β represents the FWHM of the (111) peak, and θ signifies Bragg's angle. The calculated average particle sizes vary from 14 to 15 nm. Elevated dislocation density, reduced crystallite size, and variations in d spacing induce lattice deformation. Consequently, lattice flaws arise, resulting in significant active sites with an enhanced surface area [36]. The structural parameters derived from XRD patterns are summarized in Table 3.

Table 3. *Diffraction parameters for NiCo thin films revealed from XRD analysis*

Samples	*d* / nm			*a* / nm	*D* / nm	$\delta \times 10^{-3}$ / nm^{-2}	$\varepsilon \times 10^{3}$
	111	200	220				
NiCo A	0.204066	0.176887	0.124967	0.353452	15.53	4.15	5.89
NiCo B	0.203716	0.176385	0.124766	0.352846	14.46	4.78	6.32
NICo C	0.203541	0.176306	0.124639	0.352544	14.03	5.08	6.50

In addition, we investigated the structural properties of the electrodeposited NiCo by means of Raman spectroscopy. Figure 2 shows the Raman spectra of NiCo thin films. Raman peaks found at approximately 302 and 365 cm^{-1} are attributed to phonons attached to In_2O(bcc) structures [37]. The Raman signal of 465 cm^{-1} is consistent with the A_{tg} (T) stretching mode of the Ni-O resonance vibration, while the peak of 520 cm^{-1} is consistent with the Co-O stretching mode (F_{2g}) [38]. The peak at 803 cm^{-1} corresponds to the Raman shifts of ITO [39]. Small peak around 1335 cm^{-1} corresponds to D-band carbon peak from PET [40].

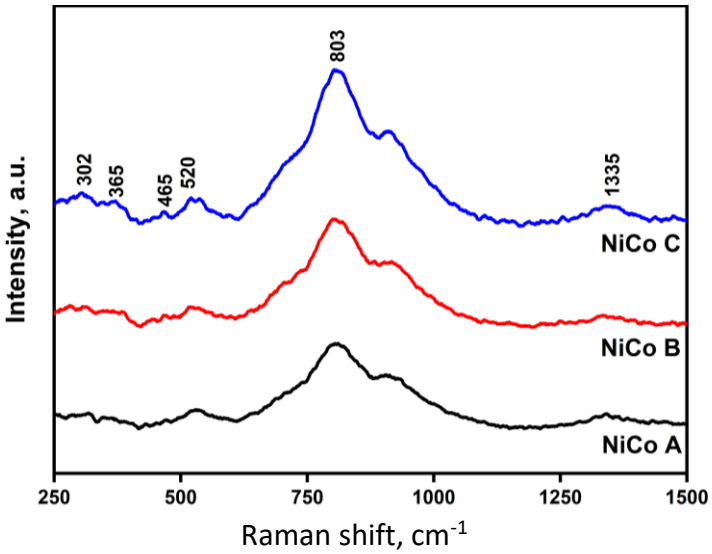

Figure 2. *Raman spectra of NiCo thin films*

Figure 3 shows the EDX spectra of the electrodeposited NiCo thin films. All three spectra clearly show significant peaks associated with cobalt and nickel, which confirm the efficient reduction of the Co^{2+} and Ni^{2+} ions and the consequent deposition of the nickel- cobalt alloy on the ITO substrate.

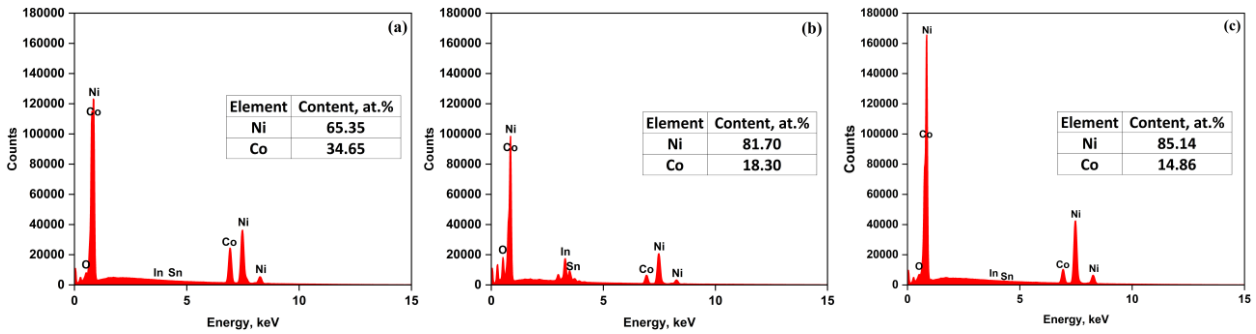

Figure 3. *EDX spectra of (a) NiCo A, (b) NiCo B, (c) NiCo C thin films*

In addition, small peaks corresponding to indium, tin and oxygen elements are also observed in the ITO substrate. The elemental composition determined by EDX is consistent with the XRD findings, in particular with the presence of a phase of FCC. These data collectively confirm the compositional variance within the films, which is closely related to the observed structural transitions.

Figure 4 shows FESEM images which clearly show how the surface structure of NiCo electrodeposited film is changing with different chemical compositions. At higher concentrations of Co, the film has a pebbly shape (Figure 4a) [41]. If there is less Co, the surface shape changes to a round shape, which is particularly noticeable in Ni-rich NiCo thin films (Figure 4b and 4c). This gradual morphological change from pebbly to round grains is attributed to changes in the crystalline structure of the film. The pebbly morphology indicates a composite phase of FCC and HCP, while the rounded structure indicates the presence of a single phase of FCC. These morphometric and structural links are consistent with previous research showing similar trends [29]. The change in surface texture indicates that cobalt is important in preventing clumping and in strengthening the bimetallic NiCo system.

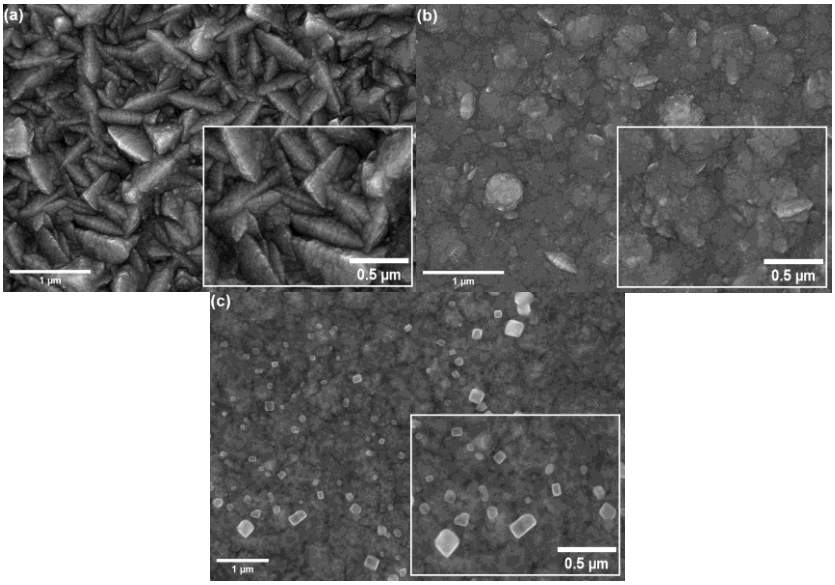

Figure 4. *FESEM micrographs of (a) NiCo A; (b) NiCo B; (c) NiCo C thin films*

Electrochemical impedance spectroscopy (EIS) was used to assess the charge transfer resistance (R_{ct}) of NiCo thin films and provide an insight into the electron transport kinetics of the NiCo thin films during EOR, which are presented in Nyquist plots shown in Figure 5.

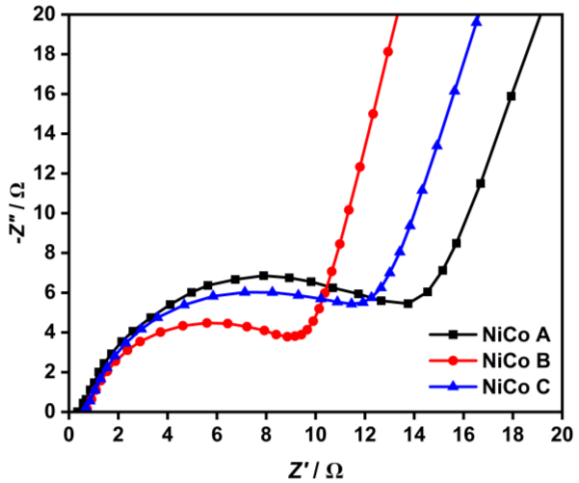

Figure 5. *Nyquist plots of NiCo thin films in 1 M ethanol + 1.0 M NaOH at 1.67 V* vs. *RHE*

The R_{CT} values for NiCo A, NiCo B and NiCo C were 15.164, 10.498 and 13.630 Ω, respectively. NiCo B has the lowest value, which indicates enhanced electron transport kinetics and conductivity due to reduced internal electrode resistance by reduced ion diffusion pathways [42]. The perfor-

mance is due to the single phase of the NiCo B FCC, which provides better electrical conductivity and less defect or grain boundary dispersion than the mixed phase NiCo A FCC and HCP [35].

Figure 6 shows the cyclic voltamograms for NiCo thin films in 1.0 M NaOH + 1 M ethanol solution. Unlike platinum-based catalysts, which typically have clear anodic peaks, all NiCo electrodes have broad-band currents without sharp anodic peaks. This suggests that oxidation of ethanol to NiCo occurs by a more continuous oxidation pathway rather than by sequential adsorption and desorption of intermediates. At higher potentials, especially at 1.8 V *vs*. RHE, where the catalyst surface is fully activated, NiCoB exhibits a peak current density of 14.82 mA cm^{-2}. This value is approximately 2.04 times and 1.33 times higher than the respective values for NiCo A (7.25 mA cm^{-2}) and NiCo C (11.11 mA cm^{-2}). The exceptional performance of NiCo B may be related to the ideal synergy between Ni, which produces the active oxygen species (NiOOH) for ethanol oxidation, and Co, which improves electronic conductivity and structural stability, thus increasing the electron transport and the efficiency of the ethanol oxidation reaction [22]. The onset potential, which indicates the point at which the current starts to increase from the beginning [43] is observed at approximately 1.35 V for NiCo B. This value is lower than that of NiCo A at around 1.40 V and NiCo C at about 1.42 V, suggesting that NiCo B promotes ethanol oxidation with greater efficiency. The combination of the lowest initial potential and the highest current density observed for NiCoB confirm its extraordinary electrochemical activity in the oxidation of ethanol. The improved performance of NiCo B is attributed to its ideal atomic ratio of Ni:Co (81:19), which balances the formation of $Ni(OH)_2$ and NiOH active sites with the bifuctional effect of Co, which increases adsorption of OH^- and facilitates oxidation of Ni. Conversely, NiCo C, which has a slightly higher Ni content (85 at.%), contains a lower Co content to facilitate this action, resulting in an increase in R_{ct} and lower current density [44].

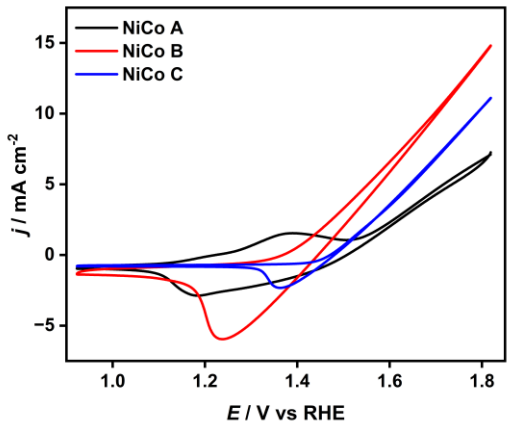

Figure 6. *Cyclic voltamogram of NiCo thin films in 1 M ethanol + 1.0 M NaOH*

A Tafel analysis was performed to determine the kinetic parameters of ethanol oxidation at NiCo thin films. Figure 7b shows the Tafel plots resulting from the LSV analysis of 1 M ethanol + 1.0 M NaOH solution on NiCo A, NiCo B and NiCo C, respectively. Tafel slopes (*b*) are defined by the Equation (7) [45]:

$$b = \frac{2.303RT}{\alpha F} \tag{7}$$

In this equation the constants *R* and *F* are universal gas constant and the Faraday constant, respectively, *T* / K is the temperature and α is the charge transfer coefficient of the reaction.

For NiCo A, B and C, the corresponding Tafel slopes were 188, 156 and 167 mV dec^{-1}, respectively. The lowest Tafel slope obtained indicates the most optimal kinetic properties attributable to the accelerated kinetic energy transfer process [24]. Consequently, the data collected indicate that NiCo B is sufficient as an electrocatalyst to enhance the oxidation reaction of ethanol [46].

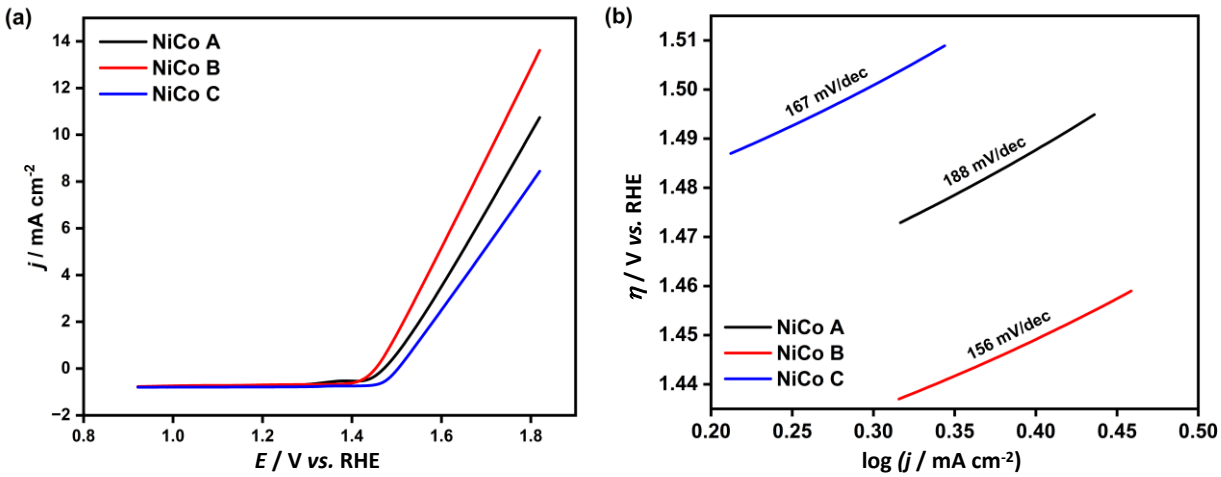

Figure 7. *(a) LSV curves and (b) Tafel plots of NiCo thin films in 1 M ethanol + 1.0 M NaOH*

The corresponding charge transfer coefficients (α) were determined using the Tafel equation, considering a four-electron transfer process in ethanol oxidation reaction. The calculated α values were 0.079, 0.095 and 0.088 for NiCo A, NiCo B, and NiCo C, respectively. NiCo B shows the highest α, consistent with its lowest Tafel slope. This confirms that NiCo B possesses the most efficient charge transfer characteristics and kinetic properties, making it the most effective catalyst among the samples.

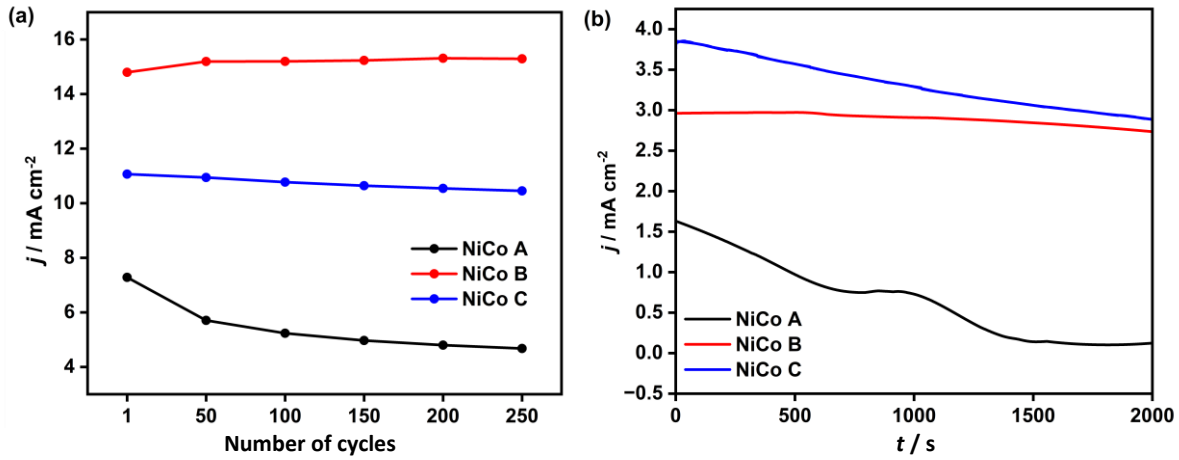

Figure 8. *(a) Long-term stability over 250 cycles at 1.80 V* vs. *RHE and (b) chronoamperometry at 1.67 V* vs. *RHE of NiCo thin films*

The long-term durability of catalysts has been acknowledged as a significant parameter in ethanol oxidation reactions [47]. We also evaluated the long-term stability of as prepared catalysts through repeated CV scan for 250 cycles and CA for 2000 s at 1.67 V *vs.* RHE in 1 M ethanol in 1.0 M NaOH. Figure 8a displays the current density for EOR as a function of the number of cycles at potential 1.8 V *vs.* RHE. As the cyclic scanning process continues, the ethanol is progressively consumed, particularly near the catalyst surface. This results in concentration polarization and a reduction in ethanol oxidation current [48]. The current density for the NiCo A catalyst decreases by 35.81 %, from 7.283 mA cm^{-2} at the first cycle to 4.675 mA cm^{-2} during the 250th cycle. Nonetheless, for NiCo B and C, the reduction in anodic current density is comparatively negligible. Specifically, for the NiCo B, there is a slightly increase in current density as the cycle progresses up to cycle 200. The NiCo B catalyst exhibits remarkable stability, with the current density declining from 15.311 mA cm^{-2} at the 200th cycle to 15.292 mA cm^{-2} at the 250th cycle, reflecting a negligible decrease of merely 0.12 %. The NiCo C catalyst exhibits a markedly lesser reduction compared to NiCo A, with a fall of only 5.30 % from 7.283 mA cm^{-2} at the first cycle to

4.675 mA cm^{-2} at the 250th cycle. The diminished currents during continuous potential cycles are linked to the poisoning of electrocatalysts by the generated intermediates and/or the reduction of ethanol concentration in the electrolyte [49]. Figure 8b presents chronoamperometric measurements conducted at potential of 1.67 V *vs.* RHE to further assess the stability of the synthesized catalysts. NiCo A and NiCo C exhibited a reduction in current density, although NiCo B remained relatively steady. As the conclusion of the experiment, the current densities remain at 7.36, 91.92 and 75.46 % for NiCo A, NiCo B, and NiCo C, respectively. The results demonstrate that NiCo B exhibited the greatest stability over extended operation, followed by NiCo C, but NiCo A experienced significant performance degradation. The outcome aligns with the previously referenced repeated CV scan, further supporting that the NiCo B catalyst exhibits superior long-term stability.

The ethanol electrooxidation reaction on the NiCo catalysts is followed by a series of stages, including ethanol adsorption, intermediate formation and degradation. The same pathway also occurs on Co surfaces. On the surface of Ni, Ni(OH) is oxidized to NiOH, which can then be oxidized to ethanol and acetaldehyde, or further oxidized to acetaldehyde and to acetic acid. Dehydrogenation of ethanol by cleavage of the O-H bond yields the ethoxy group (CH_3CH_2O), which is then oxidized to acetaldehyde (CH_3CHO) and finally to acetate ions (CH_3COO^-) [40,41]. When the water activation potential of cobalt is reduced, $(OH)_{ads}$ are made more soluble and the active layer of NiOOH is exposed, thereby increasing the catalytic activity. The mechanism of EOR at the surface of Ni in alkaline solutions is given by Equations (8) to (13), and the Co surface reaction follows the same pathway as Ni [50]:

$$Ni + 2OH^- \rightarrow Ni(OH)_2 + 2e^- \quad (8)$$

$$Ni(OH)_2 + OH- \rightarrow NiOOH + H2O + e^- \quad (9)$$

$$2NiOOH + CH_3CH_2OH \rightarrow 2NiOOH\text{-}(CH_3CH_2OH)_{ads} \quad (10)$$

$$2NiOOH\text{-}(CH_3CH_2OH)_{ads} \rightarrow CH_3CHO + 2Ni(OH)_2 + 2e^- \quad (11)$$

$$2NiOOH + CH_3CHO \rightarrow 2NiOOH\text{-}(CH3CHO)_{ads} \quad (12)$$

$$2NiOOH\text{-}(CH_3CHO)_{ads} \rightarrow CH_3COOH + Ni(OH)_2 + 2e^- \quad (13)$$

Finally, we compare the ethanol oxidation reaction activity response of the synthesized catalyst with previous study (Table 4). The data shows that the NiCo catalysts in this study have higher electrocatalytic activity.

Table 4. *Comparison of catalytic activity of the synthesized NiCo catalysts with some previous studies*

Samples	Structure	Ni:Co atomic ratio	j_p / mA cm^{-2}	Ref.
NiCo A	HCP+FCC	65:35	7.25	This study
NiCo B	FCC	82:18	14.82	
NICo C	FCC	85:15	11.11	
NiCo-LDH@CNTs-2 %	LDH	72:28	3.7	[51]
NiCo-LDH@CNTs-2.5 %	LDH	73:27	11.5	
NiCo-LDH@CNTs-3 %	LDH	68:32	3.0	
NiCo/Cu	FCC	71:29	3.14	[52]
CoNi/Cu	FCC	19:81	2.31	[53]
CoNi/Cu	FCC	30:70	1.05	
CoNi/Cu	FCC	50:50	1.21	

Conclusions

In summary, NiCo catalyst thin films have been successfully synthesized by electrodeposition, and performed studies have shown that composition of the thin films has a significant influence on the structure and the catalytic efficiency. When the amount of cobalt is reduced, the material changes from a mixture of FCC and HCP structures to only FCC structures and its shape changes from

a pebbly to a rounded form. Among all the samples, NiCo B, showed the highest oxidation efficiency of ethanol in the alkaline solution. This excellent performance is due to the single-phase FCC structure and the balanced Ni-Co ratio, which give the lowest resistance to charge transfer, the highest current density and the best stability. These findings highlight the importance of controlling the phase composition and elemental ratios to optimize the electronic structure and catalytic performance of NiCo thin films, and identify NiCo B as a highly efficient, stable and cost-effective catalyst for ethanol electrooxidation reaction.

Conflicts of interest: *The authors declare no competing financial interest.*

Acknowledgements*: This work was financially supported by the Indonesia Endowment Fund for Education (LPDP) through the RIIM scheme batch 2 with contract number 1/PG.02.00.PT/LPPM /V2025. The authors gratefully acknowledge the Center for Science Innovation (PIS), Indonesia, for providing electrochemical workstations used in the sample preparation and electrochemical analysis. The authors also extend their sincere thanks to the National Research and Innovation Agency (BRIN), Republic of Indonesia, for facilitating structural and morphological characterizations through XRD, Raman and FESEM-EDX analysis.*

References

[1] B. C. Ong, S. K. Kamarudin, S. Basri, Direct liquid fuel cells, *International Journal of Hydrogen Energy* **42** (2017) 10142-10157. https://doi.org/10.1016/j.ijhydene.2017.01.117

[2] J. Zhan, M. Cai, C. Zhang, C. Wang, Synthesis of mesoporous $NiCo_2O_4$ fibers and their electrocatalytic activity on direct oxidation of ethanol in alkaline media, *Electrochimica Acta* **154** (2015) 70-76. https://doi.org/10.1016/j.electacta.2014.12.078

[3] E. S. Kazan-Kaya, M. Bayramoğlu, Investigation of ethanol fuel electrooxidation reaction on Ni-CeO_2NRs anode electrocatalyst in alkaline media, *Journal of Electroanalytical Chemistry* **927** (2022) 116982. https://doi.org/10.1016/J.JELECHEM.2022.116982

[4] B. Braunchweig, D. Hibbitts, M. Neurock, A. Wieckowski, Electrocatalysis: A direct alcohol fuel cell and surface science perspective, *Catalysis Today* **202** (2013) 197-209. https://doi.org/10.1016/j.cattod.2012.08.013

[5] R. M. Castagna, J. M. Sieben, A. E. Alvarez, M. M. E. Duarte, Electrooxidation of ethanol and glycerol on carbon supported PtCu nanoparticles, *International Journal of Hydrogen Energy* **44** (2019) 5970-5982. https://doi.org/10.1016/j.ijhydene.2019.01.090

[6] L. S. R. Silva, I. G. Melo, C. T. Meneses, F. E. Lopez-Suarez, K. I. B. Eguiluz, G. R. Salazar-Banda, Effect of temperature on the ethanol electrooxidation at PtNirich@PtrichNi/C catalyst in acidic and alkaline media, *Journal of Electroanalytical Chemistry* **857** (2020) 1-11. https://doi.org/10.1016/j.jelechem.2019.113754

[7] C. Busó-Rogero, J. Solla-Gullón, F. J. Vidal-Iglesias, E. Herrero, J. M. Feliu, Oxidation of ethanol on platinum nanoparticles: surface structure and aggregation effects in alkaline medium, *Journal of Solid State Electrochemistry* **20** (2016) 1095-1106. https://doi.org/10.1007/s10008-015-2970-0

[8] W. Yang, H. Wang, F. Fu, PdCu nanoalloys deposited on porous carbon as a highly efficient catalyst for ethanol oxidation, *Materials Chemistry and Physics* **228** (2019) 175-179. https://doi.org/10.1016/j.matchemphys.2019.02.075

[9] S. Beyhan, K. Uosaki, J. M. Feliu, E. Herrero, Electrochemical and in situ FTIR studies of ethanol adsorption and oxidation on gold single crystal electrodes in alkaline media, *Journal of Electroanalytical Chemistry* **707** (2013) 89-94. https://doi.org/http://dx.doi.org/10.1016/j.jelechem.2013.08.034

[10] T. V. M. Sreekanth, K. Yoo, J. Kim, Thorn-shaped $NiCo_2O_4$ nanoparticles as multi-functional electrocatalysts for electrochemical applications, *Journal of the Taiwan Institute of Chemical Engineers* **114** (2020) 291-299. https://doi.org/10.1016/j.jtice.2020.09.006

[11] S. Gamal, D. A. Kospa, A. A. Ibrahim, A. I. Ahmed, A. M. A. Ouf, A comparative study of α-$Ni(OH)_2$ and Ni nanoparticle supported ZIF-8@reduced graphene oxide-derived nitrogen doped carbon for electrocatalytic ethanol oxidation, *RSC Advances* **14** (2024) 5524-5541. https://doi.org/10.1039/d3ra08208c

[12] X. Guo, T. Liang, D. Zhang, M. Zhang, Y. Lin, C. Lai, Facile fabrication of 3D porous nickel networks for electro-oxidation of methanol and ethanol in alkaline medium, *Materials Chemistry and Physics* **221** (2019) 390-396. https://doi.org/10.1016/j.matchemphys.2018.09.066

[13] I. Danaee, M. Jafarian, F. Forouzandeh, F. Gobal, M. G. Mahjani, Electrocatalytic oxidation of methanol on Ni and NiCu alloy modified glassy carbon electrode, *International Journal of Hydrogen Energy* **33** (2008) 4367-4376. https://doi.org/10.1016/j.ijhydene.2008.05.075

[14] S. Yu, Y. Zhang, G. Lou, Y. Wu, X. Zhu, H. Chen, Z. Shen, S. Fu, B. Bao, L. Wu, Synthesis of NiMn-LDH Nanosheet@Ni_3S_2 Nanorod Hybrid Structures for Supercapacitor Electrode Materials with Ultrahigh Specific Capacitance, *Scientific Reports* **8** (2018) 5246. https://doi.org/10.1038/s41598-018-23642-6

[15] H. Syafei, D.G. Kurniawan, Electrodeposition of CoxNiy Thin Film and Its Catalytic Activity for Ethanol Electrooxidation, *Chemistry and Materials* **2** (2023) 14-18. https://doi.org/10.56425/cma.v2i1.50

[16] N. A. M. Barakat, F. S. Al-Mubaddel, M. R. Karim, M. Alrashed, H. Y. Kim, Influence of Sn content on the electrocatalytic activity of NiSn alloy nanoparticles-incorporated carbon nanofibers toward methanol oxidation, *International Journal of Hydrogen Energy* **43** (2018) 21333-21344. https://doi.org/10.1016/J.IJHYDENE.2018.09.196

[17] M. Motlak, N. A. M. Barakat, M. S. Akhtar, A. M. Hamza, B. S. Kim, C. S. Kim, K. A. Khalil, A. A. Almajid, High performance of NiCo nanoparticles-doped carbon nanofibers as counter electrode for dye-sensitized solar cells, *Electrochimica Acta* **160** (2015) 1-6. https://doi.org/10.1016/j.electacta.2015.02.063

[18] S. Sun, Z. J. Xu, Composition dependence of methanol oxidation activity in nickel-cobalt hydroxides and oxides: An optimization toward highly active electrodes, *Electrochimica Acta* **165** (2015) 56-66. https://doi.org/10.1016/j.electacta.2015.03.008

[19] S. Budi, R. A. Tawwabin, U. Cahyana, Afriza, M. Paristiowati, Saccharin-assisted galvanostatic electrodeposition of nanocrystalline FeCo films on a flexible substrate, *International Journal of Electrochemical Science* **15** (2020) 6682-6694. https://doi.org/10.20964/2020.07.74

[20] S. Budi, S. Muhab, A. Soeprapto, B. Kurniawan, A. Manaf, Effect of the electrodeposition potential on the magnetic properties of FeCoNi films, *Materials Science-Poland* **37** (2019) 389-394. https://doi.org/10.2478/msp-2019-0044

[21] F. Z. Bouzit, A. Nemamcha, H. Moumeni, J. L. Rehspringer, Morphology and Rietveld analysis of nanostructured Co-Ni electrodeposited thin films obtained at different current densities, *Surface and Coatings Technology* **315** (2017) 172-180. https://doi.org/10.1016/j.surfcoat.2017.02.028

[22] M. Asgari, M. G. Maragheh, R. Davarkhah, E. Lohrasbi, A.N. Golikand, Electrocatalytic oxidation of methanol on the nickel-cobalt modified glassy carbon electrode in alkaline medium, *Electrochimica Acta* **59** (2012) 284-289. https://doi.org/10.1016/j.electacta.2011.10.091

[23] Chika Shafa Maura, Muhammad Fathar Aulia, Raudhatul Hadawiyah, Wulan Kharisma Dera, Hilman Syafei, Synthesis of CoNi by Electrodeposition Technique and its Application as an Electrocatalyst for Water Splitting, *Chemistry and Materials* **2** (2023) 72-76. https://doi.org/10.56425/cma.v2i3.64

[24] S. Budi, A. Auliya, S. Winarsih, M. H. Fauzi, N. Yusmaniar, Square-wave pulse electrodeposition of gold nanoparticles for ethanol electrooxidation, *Materials Advances* **4** (2023) 5556-5563. https://doi.org/10.1039/d3ma00412k
[25] T. M. Huynh, U. Armbruster, C. R. Kreyenschulte, L. H. Nguyen, B. M. Q. Phan, D. A. Nguyen, A. Martin, Understanding the Performance and Stability of Supported Ni-Co-Based Catalysts in Phenol HDO, *Catalysts* **6** (2016) 176. https://doi.org/10.3390/catal6110176
[26] M. Y. Rafique, L. Pan, W. S. Khan, M. Z. Iqbal, H. Qiu, M. H. Farooq, M. Ellahi, Z. Guo, Controlled synthesis, phase formation, growth mechanism, and magnetic properties of 3-D CoNi alloy microstructures composed of nanorods, *CrystEngComm* **15** (2013) 5314-5325. https://doi.org/10.1039/c3ce40385h
[27] E. Blanco, A. B. Dongil, N. Escalona, Synergy between ni and co nanoparticles supported on carbon in guaiacol conversion, *Nanomaterials* **10(11)** (2020) 2199. https://doi.org/10.3390/nano10112199
[28] S. Budi, M. Takahashi, M. G. Sutrisno, W. A. Adi, Z. Fairuza, B. Kurniawan, S. Maenosono, A. A. Umar, Phases evolution and photocatalytic activity of Cu2O films electrodeposited from a non-pH-adjusted solution, *Royal Society Open Science* **10** (2023) 230247. https://doi.org/10.1098/rsos.230247
[29] U. Sarac, M. C. Baykul, Y. Uguz, Differences Observed in the Phase Structure, Grain Size-Shape, and Coercivity Field of Electrochemically Deposited Ni-Co Thin Films with Different Co Contents, *Journal of Superconductivity and Novel Magnetism* **28** (2015) 3105-3110. https://doi.org/10.1007/s10948-015-3139-x
[30] A. Karimzadeh, M. Aliofkhazraei, F. C. Walsh, A review of electrodeposited Ni-Co alloy and composite coatings: Microstructure, properties and applications, *Surface and Coatings Technology* **372** (2019) 463-498. https://doi.org/10.1016/j.surfcoat.2019.04.079
[31] L. Kaufman, H. Nesor, Coupled phase diagrams and thermochemical data for transition metal binary systems - II, *Calphad* **2** (1978) 81-108. https://doi.org/10.1016/0364-5916(78)90006-8
[32] A. Bensouilah, A. Guittoum, M. Hemmous, A. Bouremana, B. Rahal, C. Yavru, R.M. Öksüzoglu, M. Kechouane, Structure, Microstructure and Magnetic Properties of CoxNi1 0 0 − x Powders Synthesized by Hydrothermal Method, *Journal of Superconductivity and Novel Magnetism* **30** (2017) 2219-2225. https://doi.org/10.1007/s10948-017-4035-3
[33] T. Omori, K. Oikawa, J. Sato, I. Ohnuma, U. R. Kattner, R. Kainuma, K. Ishida, Partition behavior of alloying elements and phase transformation temperatures in Co-Al-W-base quaternary systems, *Intermetallics* **32** (2013) 274-283. https://doi.org/10.1016/j.intermet.2012.07.033
[34] M. Elrouby, H. M. A. El-Lateef, M. Sadek, Electrodeposited Pt nanorods on a novel flowered-like nanostructured Ni-Co alloy as an electrocatalyst for methanol oxidation, *International Journal of Hydrogen Energy* **44** (2019) 13820-13834. https://doi.org/10.1016/j.ijhydene.2019.03.261
[35] M. R. Islam, M. Rahaman, M. M. Billah, M. R. Islam, Hydrothermal synthesis of an MoS_2/MnO_2 nanocomposite: a unique 3D-nanoflower/1D-nanorod structure for high-performance energy storage applications, *Materials Advances* **5** (2024) 5307-5321. https://doi.org/10.1039/d4ma00065j
[36] R. Zhou, C. jie Han, X. min Wang, Hierarchical MoS_2-coated three-dimensional graphene network for enhanced supercapacitor performances, *Journal of Power Sources* **352** (2017) 99-110. https://doi.org/10.1016/j.jpowsour.2017.03.134
[37] S. Harinath Babu, N. Madhusudhana Rao, S. Kaleemulla, G. Amarendra, C. Krishnamoorthi, Room-temperature ferromagnetic and photoluminescence properties of indium-tin-oxide nanoparticles synthesized by solid-state reaction, *Bulletin of Materials Science* **40** (2017) 17-23. https://doi.org/10.1007/s12034-016-1352-2

[38] M. S. Vidhya, G. Ravi, R. Yuvakkumar, D. Velauthapillai, M. Thambidurai, C. Dang, B. Saravanakumar, Nickel-cobalt hydroxide: A positive electrode for supercapacitor applications, *RSC Advances* **10** (2020) 19410-19418. https://doi.org/10.1039/d0ra01890b
[39] A. H. Sofi, M. A. Shah, K. Asokan, Structural, Optical and Electrical Properties of ITO Thin Films, *Journal of Electronic Materials* **47** (2018) 1344-1352. https://doi.org/10.1007/s11664-017-5915-9
[40] A. A. Serkov, H. V Snelling, S. Heusing, T. M. Amaral, Laser sintering of gravure printed indium tin oxide films on polyethylene terephthalate for flexible electronics, *Scientific Reports* **9** (2019) 1773. https://doi.org/10.1038/s41598-018-38043-y
[41] A. Karpuz, H. Kockar, M. Alper, The effect of different chemical compositions caused by the variation of deposition potential on properties of Ni-Co films, *Applied Surface Science* **257** (2011) 3632-3635. https://doi.org/10.1016/j.apsusc.2010.11.092
[42] B. Yin, S. Zhang, Y. Jiao, Y. Liu, F. Qu, X. Wu, Facile synthesis of ultralong MnO2 nanowires as high performance supercapacitor electrodes and photocatalysts with enhanced photocatalytic activities, *CrystEngComm* **16** (2014) 9999-10005. https://doi.org/10.1039/c4ce01302f
[43] P. D. S. Correa, E. L. Da Silva, R. F. Da Silva, C. Radtke, B. Moreno, E. Chinarro, C. D. F. Malfatti, Effect of decreasing platinum amount in Pt-Sn-Ni alloys supported on carbon as electrocatalysts for ethanol electrooxidation, *International Journal of Hydrogen Energy* **37** (2012) 9314-9323. https://doi.org/10.1016/j.ijhydene.2012.03.022
[44] R. Du, Q. Zhong, X. Tan, L. Liao, Z. Tang, S. Chen, D. Yan, X. Zhao, F. Zeng, Optimized Electrodeposition of Ni2O3 on Carbon Paper for Enhanced Electrocatalytic Oxidation of Ethanol, *ACS Omega* **9** (2024) 30404-30414. https://doi.org/10.1021/acsomega.4c01658
[45] B. Xiong, Y. Zhou, Y. Zhao, J. Wang, X. Chen, R. O'Hayre, Z. Shao, The use of nitrogen-doped graphene supporting Pt nanoparticles as a catalyst for methanol electrocatalytic oxidation, *Carbon* **52** (2013) 181-192. https://doi.org/10.1016/j.carbon.2012.09.019
[46] K. Rahmani, B. Habibi, NiCo alloy nanoparticles electrodeposited on an electrochemically reduced nitrogen-doped graphene oxide/carbon-ceramic electrode: A low cost electrocatalyst towards methanol and ethanol oxidation, *RSC Advances* **9** (2019) 34050-34064. https://doi.org/10.1039/c9ra06290d
[47] Q. Zhang, T. Chen, R. Jiang, F. Jiang, Comparison of electrocatalytic activity of Pt1-: XPdx/C catalysts for ethanol electro-oxidation in acidic and alkaline media, *RSC Advances* **10** (2020) 10134-10143. https://doi.org/10.1039/d0ra00483a
[48] Z. Deng, Q. Yi, Y. Zhang, H. Nie, NiCo/C-N/CNT composite catalysts for electro-catalytic oxidation of methanol and ethanol, *Journal of Electroanalytical Chemistry* **803** (2017) 95-103. https://doi.org/10.1016/j.jelechem.2017.09.025
[49] C. Yu, Z. Yan, L. Zhu, J. Wen, H. Wang, Z. Xu, Enhanced Catalytic Performance of Bimetallic Nickel-Cobalt Loaded Low-Content Au Catalyst Toward Ethanol Electro-Oxidation, *Electrocatalysis* **7** (2016) 193-200. https://doi.org/10.1007/s12678-016-0303-4
[50] L. Yaqoob, T. Noor, N. Iqbal, A comprehensive and critical review of the recent progress in electrocatalysts for the ethanol oxidation reaction, *RSC Advances* **11** (2021) 16768-16804. https://doi.org/10.1039/d1ra01841h
[51] Y. Li, Y. Xu, C. Li, W. Zhu, W. Chen, Y. Zhao, R. Liu, L. Wang, ZIF-67-Derived NiCo-Layered Double Hydroxide@Carbon Nanotube Architectures with Hollow Nanocage Structures as Enhanced Electrocatalysts for Ethanol Oxidation Reaction, *Molecules* **28(3)** (2023) 1173. https://doi.org/10.3390/molecules28031173
[52] A. A. Fazri, A. N. Puspita, S. Ningsih, A. Auliya, Electrodeposition of CoNi Bimetallic Catalyst for Ethanol Electrooxidation Application, *Chemistry and Materials* **2** (2023) 56-60. https://doi.org/10.56425/cma.v2i3.63

[53] H. Syafei, Dwi Giwang Kurniawan, Electrodeposition of CoxNiy Thin Film and Its Catalytic Activity for Ethanol Electrooxidation, *Chemistry and Materials* **2** (2023) 14-18. https://doi.org/10.56425/cma.v2i1.50